JOURNAL OF MATERIALS SCIENCE 19 (1984) 279–290

Characterization of the microstructure of a commercial Al–Cu alloy (2 0 1 1) by differential scanning calorimetry (DSC)

C. GARCÍA CORDOVILLA, E. LOUIS
Centro de Investigación y Desarrollo de Alicante, c/o ENDASA, Apartado 25, Alicante, Spain

In this work the microstructure of a commercial Al–Cu alloy (2 0 1 1) in several metallurgical states has been studied by means of differential scanning calorimetry (DSC). The metallurgical states were chosen in such a way that the alloy contained predominantly one of the four possible phases in these alloys (i.e. GP zones and θ'', θ' and θ phases). The commercial tempers T3 and T6 have also been considered. The interpretation of the DSC curves was aided by measuring the changes in Vickers hardness and conductivity during a linear heating similar to that provided by the DSC apparatus; these studies allow, for instance, a clearer distinction between the GP (Guinier–Preston) zone dissolution peak and the θ'' phase dissolution peak. The results are compared with those obtained by other authors.

1. Introduction

In the last few years there has been a strong revival of the use of calorimetric techniques for microstructure characterization of aluminium alloys [1–17]. The aim of this great effort is to prove the potential advantages that calorimetry has over techniques (such as TEM) traditionally used for such purposes. Although most of the work has been performed on "laboratory alloys" [1–6, 9–12], lately a considerable number of studies have been done on commercial alloys [7, 8, 13–17]. This is particularly true for alloys of the 7000 series (Al–Zn–Mg and Al–Zn–Mg–Cu) [7, 13–17]. On the other hand, commercial alloys of the 2000 series (Al–Cu), having been intensively studied in their binary versions [1–6], have not received so much attention [7, 8]. It is the purpose of the present paper to study, by means of differential scanning calorimetry (DSC) and hardness and conductivity measurements, the microstructure of the extrusion alloy AA-2011 in different metallurgical states; this alloy has the special feature of containing small quantities of low melting point elements (lead and bismuth) to improve its machinability.

Precipitation in Al–Cu alloys has been intensively studied [18–24] and although some problems related to the structure of the different phases still remain to be solved [21], the sequence most widely accepted is as follows. Solid solution → GP(I) zones → θ'' phase (or GP(II) zones) → θ' phase → θ phase. Nowadays [22] as the denomination θ'' phase is preferred over GP(II) zones, we shall use GP zones for GP(I) zones and θ'' phase.

The formation of the different phases modify the properties of the alloy relevant for the present work, this is, hardness and conductivity, in the following way. Whereas the θ phase, incoherent with the α matrix, does not harden the alloy, the other three phases do, the most effective being the θ'' phase [1, 19]. The formation of GP zones decreases the electrical conductivity (σ) of the alloy (referred to the solid solution) [19, 24, 25], while the formation of θ and θ' phases leads to large increases of σ. Very few data concerning how the precipitation of the θ'' phase affects σ are available in the literature. Hirano and Iwasaki (see Fig. 7 of [1]) found for an Al–4 wt % Cu alloy that ageing at temperatures lower than 200° C leads to very small increases of σ during

0022–2461/84 $03.00 + .12

the first few hours (period of time during which the θ'' phase is preferentially formed). This result indicates that as far as conductivity changes are concerned the θ'' phase is more similar to GP zones than to the other two phases; this is consistent with the similarities between the structures of both phases found by different authors [21]. All these data will be highly useful in discussing the results of the present study.

The alloy AA-2011 is supplied commercially mainly in two tempers, i.e. T3 and T6. Although some comments will be made on the microstructure of both tempers, in this work we will be mainly concerned with metallurgical states obtained through laboratory heat treatments chosen in such a way that the alloy contained preferentially one of the four possible phases in these alloys.

2. Experimental procedures

The material used in this work has been supplied by Extrusion Products of ENDASA (Empresa Nacional del Aluminio, SA) in rods of 32 mm diameter. The alloy had been direct chill cast in billets of 203 mm diameter, preheated at 480° C and extruded to the final diameter. Its composition is given in Table I. Samples of two different sizes were prepared: (i) 32 mm diameter × 10 mm thickness specimens for conductivity and Vickers hardness measurements and (ii) 6 mm diameter × 1 mm thickness samples for DSC. The latter samples were obtained by punching 1 mm thick sheet, rolled from discs 32 mm diameter × 4 mm thickness; both operations were performed prior to solution heat treatments. DSC samples could not be obtained by machining conductivity samples [1] just after ageing, as this operation introduces deformations that might affect DSC curves [26]. On the other hand quenching rate effects are not so strong as to cause differences between the two samples used in this work. All samples were solution heat treated at 525° C for 5 h and water quenched (to room temperature) prior to any ageing heat-treatment.

Heat-treatments at temperatures lower than 200° C were carried out in thermostatically controlled oil or water baths, whereas for high temperatures an air furnace was used, the temperature control being accurate to ± 1 and ± 5° C, respectively. If measurements could not be made immediately after heat treatments, the samples were kept when needed (solution heat treated samples), in liquid nitrogen.

Conductivity was measured by means of a Sigmatest-T instrument type 2.067 and the load used to measure the Vickers hardness was 1 kg. Both properties were always measured at room temperature.

The DSC measurements were performed using a Perkin Elmer DSC-2C apparatus controlled through a mini-computer. To increase the sensitivity of the measurements high purity aluminium was used as the reference. The runs were carried out at heating rates between 2.5 and 200° C min^{-1}, from 25 to 580° C. All experiments were performed under dynamic nitrogen atmosphere (1 l h^{-1}). The interpretation of the DSC curves was aided by measuring conductivity and Vickers hardness on specimens that had been linearly heated in a sand fluidized furnace at a heating rate of 5° C min^{-1} up to different temperatures (an error of ± 2° C was estimated) and then quenched in water at room temperature. Both the DSC measurements and the linear heatings to measure σ and VH were performed at least twice; good reproducibility was found.

The metallurgical states studied in this work were chosen from the isothermal ageing studies described in the next section, and the results of other authors [1, 2, 19].

3. Results and discussion

In this section we discuss first the isothermal ageing of alloy AA-2011 at different temperatures. The results obtained through those studies helped to choose the metallurgical states to be studied by calorimetric techniques.

3.1. Isothermal ageing

The homogenized and quenched samples were aged at temperatures in the range 25–420° C. The ageing was followed by measuring conductivity (σ) and Vickers hardness (VH). The results for the temperatures chosen for the DSC studies are shown in Figs. 1 and 2.

Ageing at 25° C leads to small changes in both

TABLE I Composition of the AA-2011 alloy used in this work (in weight per cent)

Fe	Cu	Si	Mn	Ti	Zn	Cr	Pb	Bi
0.31	5.41	0.12	< 0.02	< 0.02	< 0.04	< 0.04	0.35	0.44

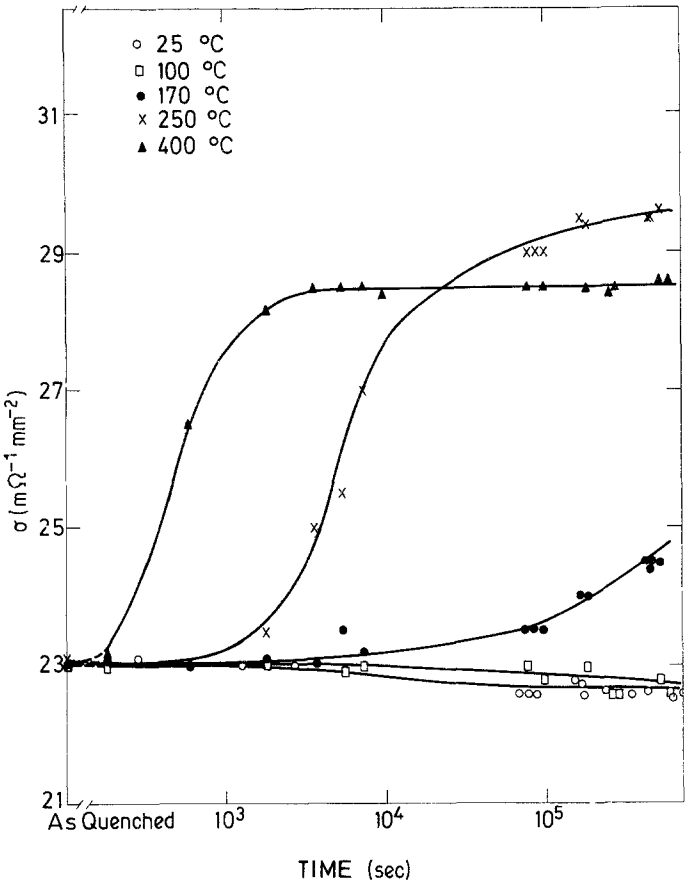

Figure 1 Change of electrical conductivity of alloy AA-2011 during ageing at different temperatures. The alloy had been homogenized at 525° C for 5 h and quenched in water at room temperature. Values for as-quenched (AsQ) samples are also given.

σ and VH [18]; the decrease in σ clearly indicates that GP zones are being formed [19, 24, 25]. The small increase in VH at 25° C does not agree with results reported by Vigier *et al.* [6] for an Al–4 wt % Cu alloy; those authors found that VH increased nearly as much as for ageing at 100° C (see below). We do not understand this disagreement, but it should not be ascribed to the presence of lead and bismuth, but rather to the microstructure of the extruded rod. At 100° C we note a strong increase of VH whereas σ remains nearly constant, although a very slight decrease (not accurately measured with the techniques used in this work) can be noticed. Again GP zones are being formed, and their larger size and the faster kinetics, with respect to those formed at 25° C, could explain the different behaviour of σ [25] and VH. These results are in agreement with those of other authors, as it is generally believed that only GP zones are formed below 130° C [1–8].

At 170° C the Vickers hardness increases strongly and for ageing times beyond 10^5 sec it slowly decreases. On the other hand σ slightly increases for ageing times shorter than 10^5 sec and more rapidly thereafter. These results indicate that beyond 10^5 sec a phase not very effective in hardening the alloy and promoting large increases in σ is being formed; this should be the θ' phase [8]. For shorter ageing times as σ slightly increases, the θ'' phase might be precipitating, although we cannot conclude whether or not for very short times the GP zones are being formed (see results for ageing at 190° C in [8]).

Ageing at 250° C indicates that for times shorter than 10^4 sec the θ' phase is formed and for longer times the incoherent θ phase starts to precipitate (see Fig. 2). The ageing at 400° C leads to the formation of the θ phase as the decrease of VH and increase of σ clearly indicate (VH is higher in the solution treated state than in the annealed state).

To summarize these results we quote temperatures and times used to obtain metallurgical states having predominantly one precipitate phase. For GP zones both 25 and 100° C temperatures were chosen, the ageing times being 7 days and 24 h, respectively. Samples containing the θ'' or θ' phase

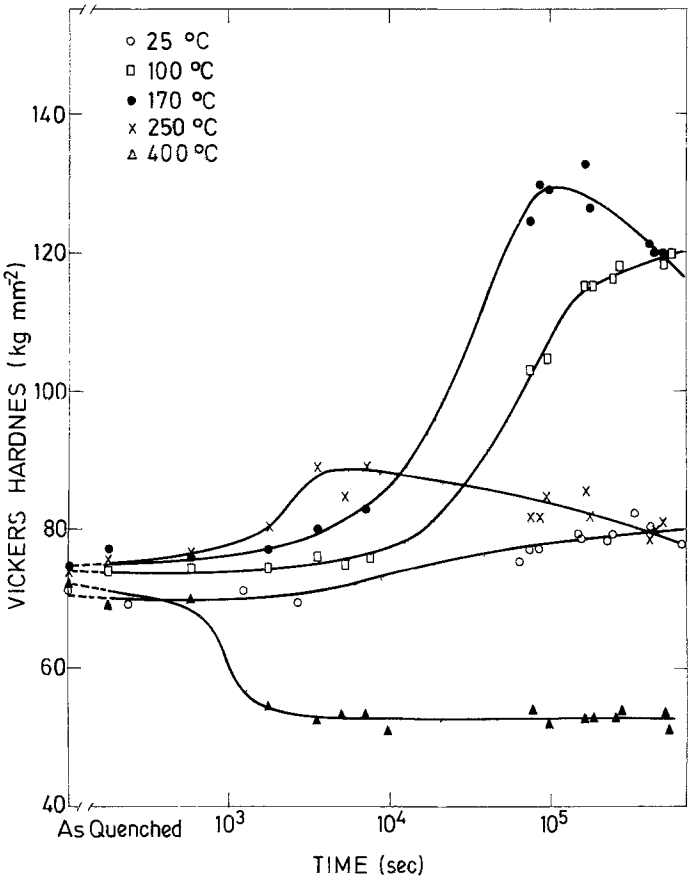

Figure 2 Same as Fig. 1 for Vickers hardness (VH). The variation in VH values for as-quenched samples ($< 4\,kg\,mm^{-2}$) is within the error usually found in commercial alloys.

were obtained by ageing 24 h at 170° C or 5 h at 250° C. The fully annealed stated (only θ phase) was achieved by ageing during 6 h at 400° C and slowly cooling to room temperature.

3.2. Calorimetric studies

3.2.1. Fully annealed state, ageing at 400° C (Fig. 3)

We noted a single endothermic reaction in the DSC curve. This reaction is clearly related to the dissolution of the only phase present in this state (see above and [1–8]). This interpretation is supported by the conductivity and Vickers hardness results shown in Fig. 3b. In this figure we note that σ starts to decrease and VH to increase roughly at the same temperature that the onset of the DSC reaction occurs. Finally we notice a weak endothermic peak at around 127° C that is related, as discussed below, to Pb–Bi particles.

3.2.2. Ageing at 250° C (Fig. 4)

In this case the DSC curves show two endothermic reactions overlapping with an exothermic reaction; these reactions should be related with θ' and θ dissolution and θ phase formation, respectively. Again this interpretation is confirmed by the VH and σ results (Fig. 4b). Roughly coinciding with the onset of the first endothermic reaction both VH and σ decrease indicating that the θ' phase is being dissolved. Between 350 and 400° C both VH and σ remain nearly constant. In this region the dissolution of the θ' phase is balanced by the formation of the θ phase. This is noticed in the DSC curve as the region where the exothermic reaction predominates. For higher temperatures σ decreases monotonically down to the value corresponding to the solution treated state, whereas VH first decreases and beyond 450° C it starts to increase indicating that the dissolution of the θ phase predominates (see the DSC curve).

3.2.3. Ageing at 170, 100 and 25° C (Figs. 5 to 8)

In this subsection we face the problem of distinguishing between GP zones and the θ'' phase.

We discuss first the case of 170° C (Fig. 5). In this case, in addition to the reactions found in samples aged at 250° C we note two more peaks,

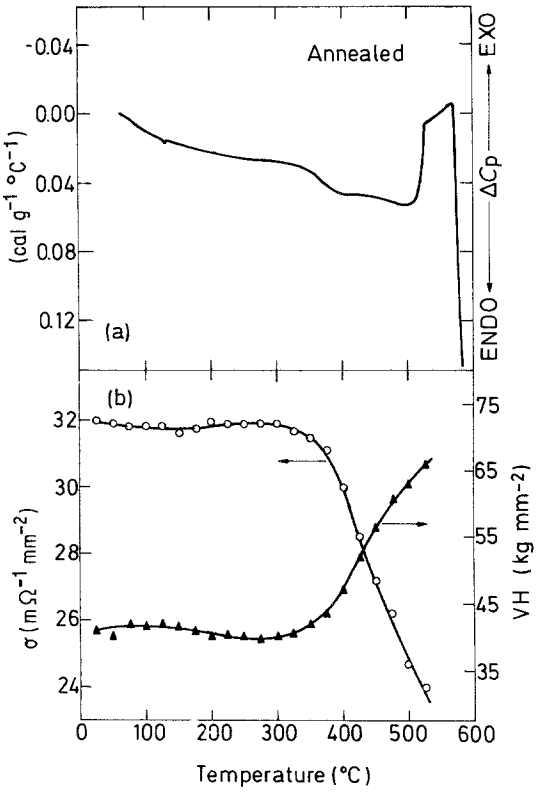

Figure 3 (a) DSC curve (heating rate 5° C min^{-1}), and (b) change of conductivity (σ) and Vickers hardness (VH) during linear heating at 5° C min^{-1}, for alloy AA-2011 annealed at 400° C for 6 h and slowly cooled.

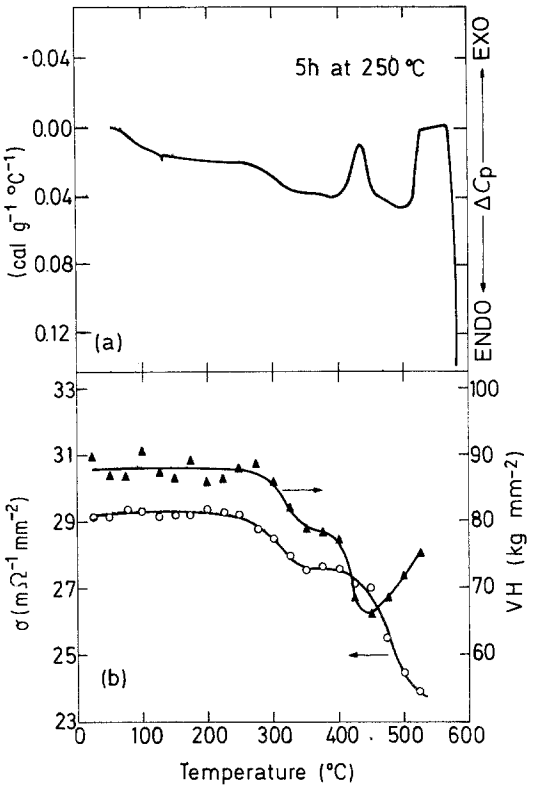

Figure 4 Same as Fig. 3 for samples aged at 250° C for 5 h.

one endothermic reaction whose maximum occurs at 228° C (see Table II for variation of this maximum with heating rate) and an exothermic reaction with its maximum lying at 310° C (see Table III). In Fig. 5b we show the variation of Vickers hardness and conductivity. VH starts to decrease when the reversion of the θ'' phase starts (first endothermic reaction); it goes down to a weak minimum, increases slightly and finally decreases to the solid solution values. As the weak minimum is above the solid solution value, it can be concluded that not all θ'' phase particles are dissolved. This suggests that the θ' phase can either be formed through transformation of the θ'' phase or directly from the solid solution; whereas the first process would decrease VH, the second increases it, and this competition might be the reason for the weak relative maximum in VH. Nonetheless, as the maximum occurs 20° C below the maximum of the exothermic reaction, it might also be concluded that the coherency of the θ' phase with the α matrix, decreases as the temperature increases. The formation of the θ' phase during the exothermic reaction is indicated by the fact that the latter part of the DSC curve is very similar to that corresponding to samples aged at 250° C. σ remains nearly constant up to 300° C, when the θ' phase starts to be formed then increases steadily, and when the exothermic reaction ends, it decreases indicating the dissolution of the θ' phase. In this temperature region

TABLE II DSC peak temperature (° C) for the first endothermic reaction of samples aged at 100 and 170° C for different heating rates

Peak temperature (° C)	Heating rate (° C min^{-1})				
	5	20	40	100	200
100	170	186	196	205	222
170	228	243	253	262	270

TABLE III Same as Table II for the main exothermic peak (θ' phase precipitation)

Peak temperature (° C)	Heating rate (° C min^{-1})			
	2.5	5	20	40
100	323	336	372	388
170	303	319	368	379

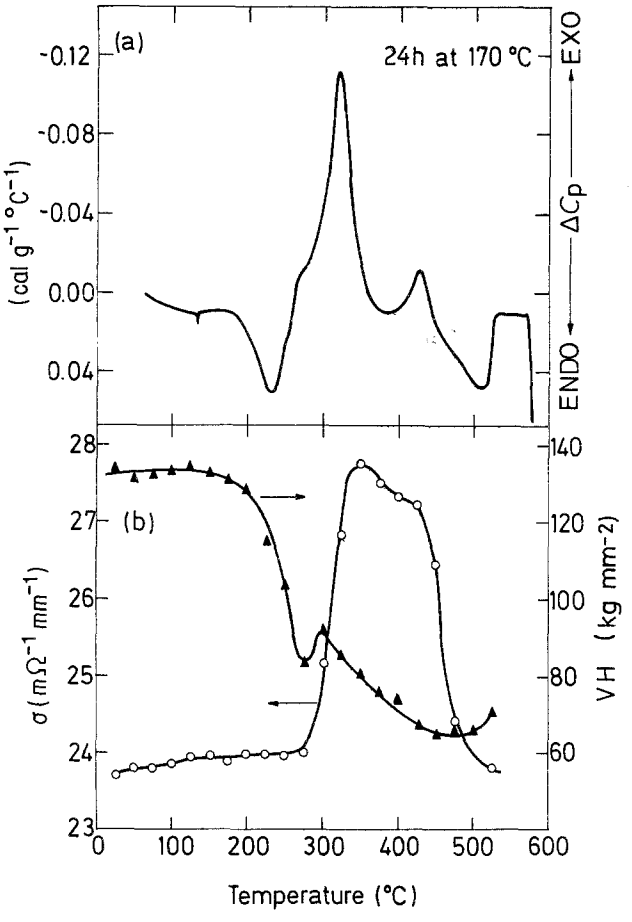

Figure 5 Same as Fig. 3 for samples aged at 170° C for 24 h.

the latter process competes with the formation of the θ phase and therefore σ varies very slowly; it starts to decrease very rapidly at the onset of the last endothermic reaction. The fact that below 300° C σ remains constant and does not go down to the as-quenched value might also support the assumption that not all θ'' phase particles are dissolved; nonetheless the not very high accuracy of our σ measurements questions this conclusion. All these results indicate that the first endothermic peak is related to reversion of the θ'' phase whereas the exothermic peak corresponds to the formation of the θ' phase.

We turn now to consider the case of 100° C (Fig. 6). The DSC curve is similar to the one previously considered but the first endothermic peak is shifted 58° C downwards (Table II) whereas the exothermic peak shifts 17° C upwards (Table III). The VH starts to decrease at the onset of the first endothermic reaction and it attains the solid solution value before it increases again. This indicates that most GP zones are dissolved before the θ' phase starts to be formed, (above 300° C). At the end of the first endothermic reaction σ has increased above its solid solution value; this suggests that at the end of this peak, some other reactions might be superimposed on to the dissolution of GP zones. Above 300° C the behaviour of VH and σ is rather similar to the previous case; slight differences might be explained by the different balance between the dissolution of the θ' and θ phases and the formation of the latter.

Although the VH results already differentiate between the GP zones and the θ'' phase, we have made two further studies. First we have obtained a DSC curve of both samples (aged at 100 and 170° C) at a low heating rate (2.5° C min^{-1}). The outstanding differences between them are readily noticed (Fig. 7). Whereas in the 170° C case, below 300° C there is a single endothermic reaction (a small shoulder might be indicating that some growth of the θ'' phase takes place), in the 100° C case there are two reactions in between the dissolution of the GP zones and the formation of the θ' phase. As first pointed out by Zahra *et al.*

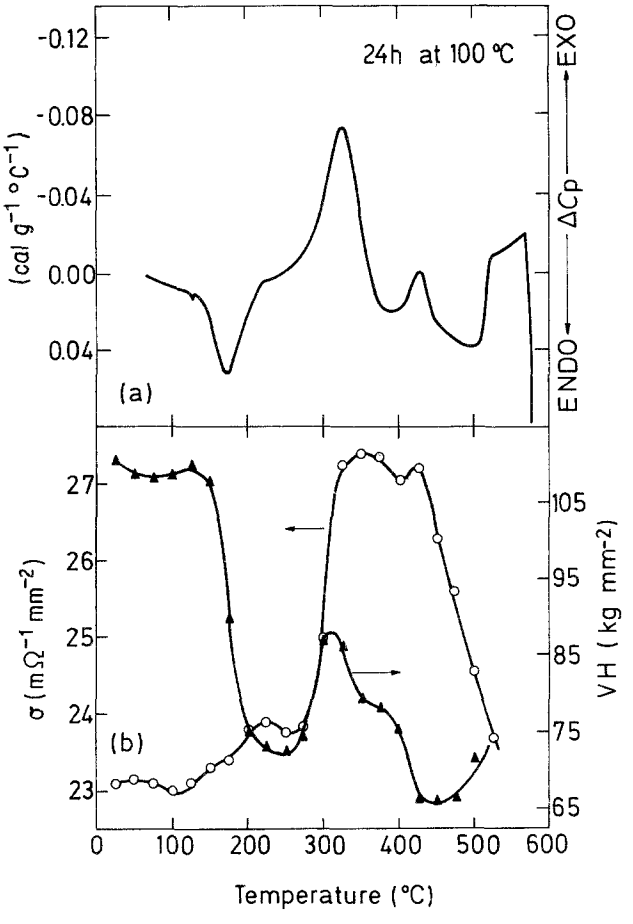

Figure 6 Same as Fig. 3 for samples aged at 100° C for 24 h.

[3], for low heating rates, the θ'' phase might be formed and dissolved during the linear heating, just after GP zones dissolution and before the exothermic peak. As a second study we have obtained the activation energy of both dissolution peaks (GP zones and the θ'' phases). To this end we have used the so-called "peak method" first introduced by Kissinger [27] and Henderson [28]. This method is based upon the assumption that the peak of the DSC curve coincides with the maximum reaction rate; although this assumption is not valid for differential thermal analysis [29] it holds for DSC [30]. By assuming a Johnson–Mehl–Avrami equation for the reaction rate [28] the following equation is obtained at the peak of the DSC curve [27, 28].

$$\ln \frac{h}{T_p^2} = -\frac{E}{RT_p} + \ln \frac{\nu R}{E} \qquad (1)$$

where T_p is the temperature at the peak, h the heating rate, R the gas constant and E and ν the kinetic parameters in the Arrhenius equation, that is the activation energy and frequency factor, respectively. Equation 1 holds no matter the value of the reaction order n. By varying the heating rate, Equation 1 can be used to obtain E and ν. For obtaining the reaction order n a fitting of the full DSC curve should be made [7]. In the calculation of E and ν we have used the peak temperatures given it Table II. The peak temperatures at 2.5° C min^{-1} have not been included, as the DSC curve at this heating rate is markedly different from those at higher heating rates. For a similar reason the peak temperatures for the formation of the θ' phase at 200° C and 100° C min^{-1} have not been quoted in Table III, as at high heating rates the θ phase is formed instead of the θ' phase. The activation energies obtained for ageing at 100 and 170° C are 1.27 and 1.89 eV molecule^{-1}, respectively. In comparing the present values for E and ν with those reported in the literature it should be noted that E and ν depend upon the equation chosen for the reaction rate [7]. Papazian [7] by using the same equation

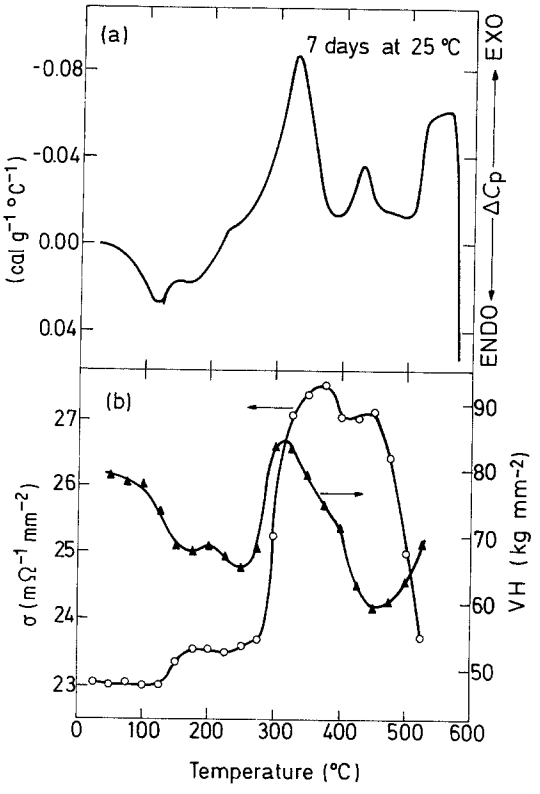

Figure 7 DSC curves of samples aged at 100° C (continuous line) and 170 (broken line) for 24 h; heating rate of 2.5° C min^{-1}.

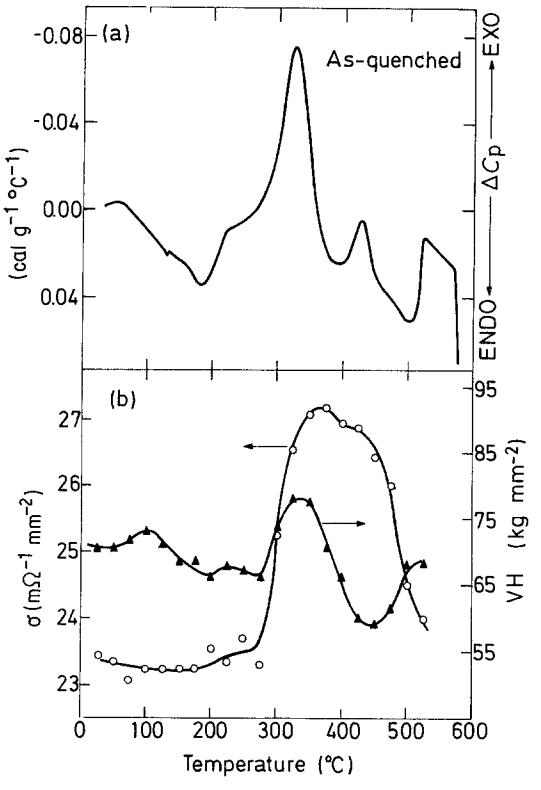

Figure 8 Same as Fig. 3 for samples aged at 25° C for 7 days.

for the reaction rate as here obtained 0.83 eV molecule^{-1} for dissolution of GP zone formed at room temperature (T31 temper); other values lie in the range 1.0–1.3 eV molecule^{-1} [18]. Although in the model herewith assumed (a Johnson–Mehl–Avrami equation for the reaction rate) the activation energy might increase as the size of the GP zone increases (large zones for higher ageing temperature, see [7]), the large E obtained here for ageing at 170° C (note that 1.89 eV molecule^{-1} is well above the upper end of the range reported in the literature) suggests that a different phase is formed at this temperature. Nonetheless a more detailed study, of the kinetics of dissolution of GP zone or θ'' phase formed at different ageing temperatures is required before reaching a definitive conclusion.

Before ending the discussion of ageing at these two temperatures we remark on two further points, (i) the formation of the θ' phase depends on the history of the sample, that is, it is not the same for the two ageing temperatures (see Table II) and, (ii) the temperature of the maximum of the θ phase dissolution peak is roughly the same for the two ageing temperatures and depends on heating rate (Table IV) to a lesser extent that those corresponding to other reactions (Tables II and III), remaining constant for heating rates up to 40° C min^{-1}.

Finally we discuss briefly the case of ageing at 25° C (Fig. 8). The only noticeable differences with the results for ageing at 100 and 170° C occur below 300° C. For instance we notice that the GP zone dissolution peak is not as simple as that of ageing at 100° C. First it starts at lower temperatures and second it shows a strong shoulder just below 200° C. The earlier start of the GP zone dissolution reaction indicates the lower stability (smaller size) of the GP zone formed at 25° C with

TABLE IV Same as Table II for dissolution of the θ phase

Peak temperature (° C)	Heating rate (° C min^{-1})					
	2.5	5	20	40	100	200
100	505	505	504	512	523	528
170	505	504	504	511	519	523

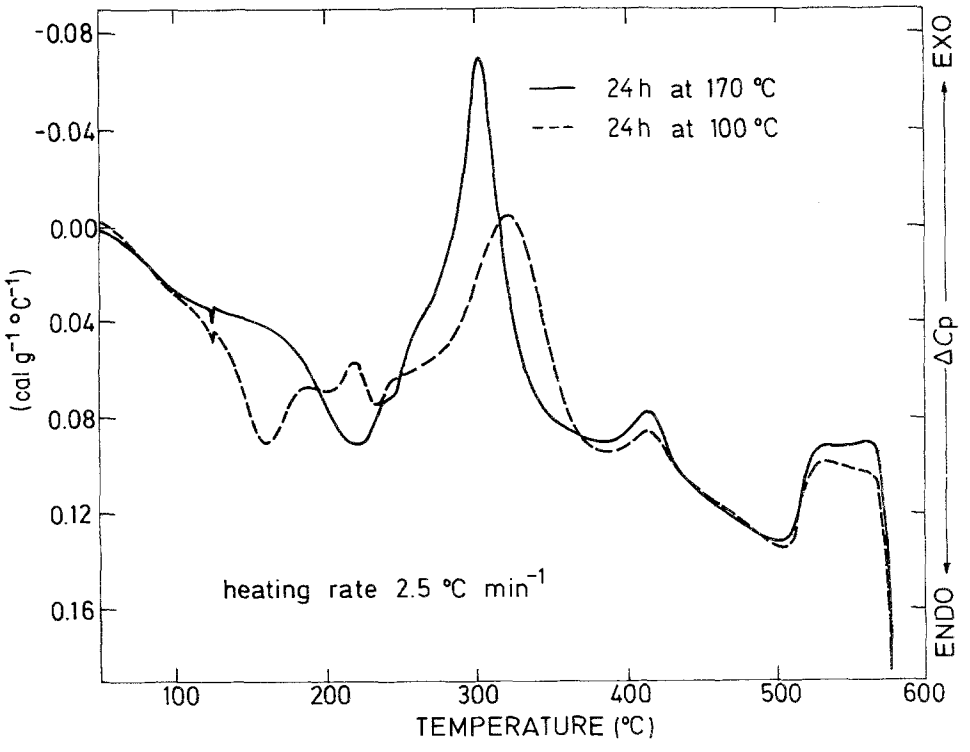

Figure 9 Same as Fig. 3 for as-quenched samples.

respect to those formed at 100° C. On the other hand the shoulder might be associated with GP zone growth as suggested by other authors [3]. Nonetheless the small maximum in VH at around 200° C could indicate that around this temperature two phenomena might be occurring, namely, dissolution of small GP zone formed at 25° C and formation of larger GP zones. In general we notice that the GP zone dissolution peak is much narrower for samples aged at 100° C than for those aged at 25° C, indicating a more uniform size distribution.

3.2.4. As-quenched sample (Fig. 9)

Above 300° C the DSC curves and results for VH and σ are again very similar to those corresponding at samples aged at 100 and 170° C. Below this temperature we notice in the DSC curve an exothermic reaction below 100° C. This would be related with formation of GP zone. These GP zones are then dissolved leading to the first endothermic reaction. We notice that these GP zones are mostly formed at temperatures close to 100° C; this is the reason why the dissolution peak is closer to that of GP zones formed at 100° C rather than at 25° C. The VH and σ results clearly support the above interpretation. The VH first increases (up to 100° C) and afterwards decreases (dissolution of GP zones), whereas σ decreases (formation of GP zones) and during dissolution it increases again.

3.3. Commercial tempers

In this work only two commercial tempers have been considered, namely, T3 and T6. The former has been obtained by deforming the sample 3% just after solution heat treatment and subsequent ageing at 25° C during 7 days; as the 3% stretching was performed on 50 mm x 20 mm x 1 mm samples it was then necessary to punch DSC samples from the sheet; thus, as punching might also introduce some deformation [26], a sample punched just after ageing from a non-stretched sheet was also prepared. In Fig. 10 the DSC curves for the T3 temper and the two more samples, one with no plastic deformation and another punched from unstretched sheet just after ageing, are shown. In comparing DSC curves for stretched-punched samples with those corresponding to samples with no plastic deformation, two points are worth noticing: (i) the GP zones dissolution peak is at higher temperatures for the T3 temper and is narrower, and (ii) the θ' formation peak (main exothermic reaction) is at much lower tempera-

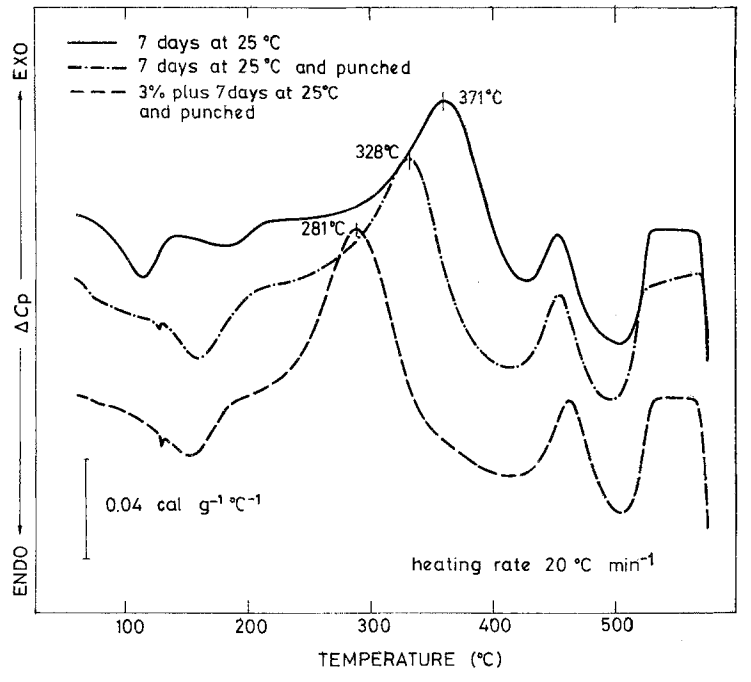

Figure 10 DSC curves for samples stretched 3% and naturally aged at 25° C for 7 days (T3 heat treatment) and punched (continuous line), punched and unstretched samples (chain line) and samples with no plastic deformation (unpunched and unstretched). Heating rate 20° C min^{-1}.

tures for the T3 temper than for samples without plastic deformation (see Fig. 10). These results indicate that (a) GP zones formed after plastic deformation are larger and their size distribution is more uniform; the effect of cold work is, as suggested elsewhere [8, 20], to favour the freeing of vacancies from sinks, and this mechanism might accelerate GP zones formation, and (b) cold work accelerates θ' formation, this is readily explained by the fact that dislocations might act as nucleation sites for θ' particles [20]. We also notice that as the θ' phase formation is accelerated so is its dissolution, although formation and dissolution of the θ phase are not greatly affected by deformation. Finally it is worth remarking that the punching operation adds deformation to the 3% stretching. Therefore the actual shift of the exothermic peak due to the 3% deformation should be the difference between the shift corresponding to punched samples (43° C) and that for stretched (punched also) samples (90° C), this turns out to be around 47° C.

The T6 commercial temper is obtained by artificially ageing the alloy at temperatures in the range 170–190° C. As it is common to have a delay time at room temperature between the solution heat treatment and the artificial ageing, we have studied the effect of this natural ageing. To this end we have made calorimetric studies of samples kept at 25° C during 7 days before an artificial ageing at 170° C for 24 h, and compared the results with those obtained with no natural ageing (Fig. 5). No dramatic differences are noticed between the DSC curves for both type of samples. We only notice that, for samples with natural ageing, the θ'' dissolution peak is shifted 5° C upwards, indicating a slightly larger size of the θ'' particles, and the θ' formation peak is shifted 5° C downwards, that is, the formation of the θ' phase is accelerated.

3.4. Distribution of Pb–Bi particles

In all samples analysed in this work (over 100) a weak endothermic peak at around 125° C has been found. In very few samples some other endothermic peaks between 125–300° C have also been noticed. This result indicates that most Pb–Bi particles are around the eutectic composition (56.3 wt % Pb), as the eutectic temperature is 125° C [31]. This is not surprising considering the way in which those two elements are usually added to the alloy, namely, a mixture of Pb–Bi is poured over the liquid alloy which is subsequently stirred (see Table I for composition).

3.5. Comparison with other works

In comparing our results with those obtained by other authors [1–8] some points are worth noticing.

(i) The features of the DSC curves of alloy

AA-2011 are similar to those of pure Al–Cu alloys [1–6]. Nonetheless an outstanding difference should be noted, namely, whereas in pure alloys [3] the formation of the θ' phase and the last three reactions (dissolution of the θ' and θ phases and formation of the θ phase) do not depend on the thermal history of the alloy (are the same for samples aged at 100 or 170° C), in the present alloy they do.

(ii) Papazian [8] has found for the AA-2219 alloy, that the θ' formation peak was shifted around 50° C downwards with respect to pure Al–Cu alloys [1]. He ascribed this result to trace alloying elements. As we have not found any noticeable shift of this peak, we seek for differences between Papazian's alloy and ours. The AA-2019 alloy studied by Papazian contained manganese and zirconium whereas ours does not. As zirconium should be forming insoluble $ZrAl_3$ particles, it is more likely that manganese is the element causing the acceleration of θ' formation in alloy AA-2019 [8]. The shift found by Papazian might be also due to sample preparation, as deformation introduced during punching of DSC samples could shift downwards the exothermic peak [26].

(iii) Our results concerning the microstructural effects of plastic deformation between solution heat treatment and natural ageing are rather similar to those found by Papazian [8]. Due to the higher deformation given in this work (3%) with respect to Papazian (1%), the temperature of maximum reaction rate for the formation of the θ phase is shifted, with respect to samples with no deformation, to a larger extent in the present case (47° C) than in Papazian's work (23° C); notice also the lower heating rate used by Papazian (10° C min^{-1}).

(iv) The final point concerns the dissolution of the θ phase. Papazian [7] has noted that this phase remained in thermodynamic equilibrium with the matrix in the temperature range 300 to 500° C for heating rates up to 10° C min^{-1}. This was concluded as the dissolution of the θ phase occurred at the same temperature regardless of heating rate. In Table IV we quote the peak temperature for dissolution of the θ phase for heating rates in the range 2.5 to 200° C min^{-1}. We note that this temperature remains constant for heating rates up to 20° C min^{-1}. For higher heating rates, even the rapid diffusion at these temperatures is not high enough to preserve thermodynamic equilibrium between the θ phase and the matrix.

4. Concluding remarks

The following conclusions emerge from the results of the present work.

1. Differential scanning calorimetry is a rapid and reliable tool for studying the microstructure of alloy AA-2011. It can help in the study of the distribution of Pb–Bi particles.

2. Measurements of Vickers hardness and conductivity during a linear heating similar to that provided by the DSC apparatus are of great value for the interpretation of DSC curves. In particular they aid the differentiation between dissolution of GP zones and that of the θ'' phase.

3. The general features of the DSC curves for 2011 alloy are similar to those of pure Al–Cu alloys [1–6]. The outstanding difference is the dependence of the formation of the θ' phase on the thermal history of the alloy [3] found in the present work. It can be concluded that, as expected, lead and bismuth do not affect precipitation and dissolution processes in Al–Cu alloys.

4. Comparison of the peak temperatures for the θ' phase formation found by Papazian [8] for alloy 2019 with those obtained in the present work for alloy 2011, and those found for pure alloys [1], allow us to conclude that the θ' phase formation is accelerated in Papazian's work through two possible mechanisms, (i) deformation, introduced during punching of DSC samples and (ii) manganses content of alloy AA-2219.

5. Plastic deformation between solution heat treatment and natural ageing enhances GP zone formation and strongly accelerated precipitation of the θ' phase. In the present case 3% deformation lowered the θ' phase formation peak in 47° C.

6. The stable phase (θ) remains in thermodynamic equilibrium with the matrix in the temperature range 300–530° C for heating rates up to 20° C min^{-1}.

7. For a heating rate of 2.5° C the θ'' phase is formed, after dissolution of GP zones, during the linear heating. For higher heating rates the precipitation of the θ'' is prevented.

Acknowledgement

We are grateful to J. E. Alvarez for some useful and lively discussions. We also wish to thank Alcan International Ltd for permission to publish this work.

References

1. K. HIRANO and H. IWASAKI, *Trans. Jpn. Inst. Met.*

5 (1964) 162.
2. A. ZAHRA and C. Y. ZAHRA, *Scripta Metall.* **9** (1975) 879.
3. A. ZAHRA, M. LAFFITTE, P. VIGIER and M. WINTENBERGER, *Aluminium* **52** (1976) 357.
4. *Idem, Mem. Sci. Rev. Metall.* **74** (1977) 561.
5. *Idem, C.R. Acad. Sci. Paris* **277** (1973) 923.
6. P. VIGIER, A. M. ZAHRA-KUBIK, M. DENOUX, J. P. BRISSET and M. WINTENBERGER, *Mem. Sci. Rev. Metall.* **LXIX** (1972) 51.
7. J. M. PAPAZIAN, *Metall. Trans. A* **13A** (1982) 761.
8. *Idem, ibid.* **12A** (1981) 269.
9. K. HIRANO, in "Thermal Analysis: Comparative Studies on Materials", edited by H. Kambe and P. D. Garn (Wiley and Sons, New York, 1974) p 42.
10. K. ASANO and H. HIRANO, *Trans. Jpn. Inst. Met.* **9** (1968) 24.
11. A. ZAHRA, C. Y. ZAHRA, M. LAFFITTE, W. LACOM and H. P. DESGISCHER, *Z. Metallkde.* **70** (1979) 172.
12. M. RADOMSKY, O. KABISCH, H. LÖFFLER, J. LENDVAI, T. UNGÁR, I. KOVÁCS and G. HONYEK, *J. Mater. Sci.* **14** (1979) 2906.
13. D. S. THOMPSON, in "Thermal Analysis", Vol. 2, edited by R. F. Schwenker Jr and P. D. Garn (Academic Press, New York, London, 1969).
14. D. J. LLOYD and M. C. CHATURVEDI, *J. Mater. Sci.* **17** (1982) 1819.
15. C. G. CORDOVILLA and E. LOUIS, *J. Thermal Anal.* **24** (1982) 215.
16. R. De IASI and P. N. ADLER, *Metall. Trans. A* **8A** (1977) 1177.
17. P. N. ADLER and R. De IASI, *ibid.* **8A** (1977) 1185.
18. L. E. MONDOLFO, "Aluminium Alloys: Structure and Properties" 1st edn (Butterworth, London, Boston, 1976) p. 719.
19. H. K. HARDY and R. B. NICHOLSON, Progress in Metal Physics 5 (Pergamon Press, Oxford, 1954) p. 143.
20. A. KELLY and R. B. NICHOLSON, "Progress in Materials Science" Vol. 10 (Pergamon Press, Oxford 1963) pp. 149–391.
21. V. A. PHILLIPS, *Acta Metall.* **23** (1975) 751, and references therein.
22. G. W. LORIMER, "Precipitation Process in Solids", TMS-ATM (ATM Warrendale, Pennsylvania, 1973) p. 87.
23. R. J. RIOJA and D. E. LAUGHLIN, *Met. Trans A* **8A** (1977) 1257.
24. K. ASANO and K. HIRANO, *Trans. Jpn. Inst. Met.* **13** (1972) 112.
25. P. GUYOT and J. P. SIMÓN, *Scripta Metall.* **11** (1977) 751 and references therein.
26. C. G. CORDOVILLA and E. LOUIS, *Metall. Trans. A* (1983) in press.
27. H. E. KISSINGER, *Anal. Chem.* **29** (1975) 1702.
28. D. W. HENDERSON, *J. Non-Cryst. Solids* **30** (1979) 301.
29. R. L. REED, L. WEBBER and B. S. GOTTFRIED, *Ind. Eng. Chem. Fundls.* 4 (1965) 38.
30. E. LOUIS and C. G. CORDOVILLA, *J. Mater. Sci.* (1983) in press.
31. M. HANSEN and K. ANDERKO, "Constitution of Binary Alloys" 2nd edn (McGraw-Hill, New York, 1958) p. 324.

Received 7 February
and accepted 18 May 1983